Observing Changes in the Structure and Oligomerization State of a Helical Protein Dimer Using Solid-State Nanopores

David J. Niedzwiecki,[†] Christopher J. Lanci,[‡] Gabriel Shemer,[†] Phillip S. Cheng,[‡] Jeffery G. Saven,[‡] and Marija Drndić*[,†]

[†]Department of Physics and Astronomy, University of Pennsylvania, 209 South 33rd Street, Philadelphia, Pennsylvania 19104-6396, United States and
[‡]Department of Chemistry, University of Pennsylvania, 231 South 34th Street, Philadelphia, Pennsylvania 19104-6323, United States

ABSTRACT Protein analysis using solid-state nanopores is challenging due to limitations in bandwidth and signal-to-noise ratio. Recent improvements of those two aspects have made feasible the study of small peptides using solid-state nanopores, which have an advantage over biological counterparts in tunability of the pore diameter. Here, we report on the detection and characterization of peptides as small as 33 amino acids. Silicon nitride nanopores with thicknesses less than 10 nm are used to provide signal-to-noise (S/N) levels up to S/N ~ 10 at 100 kHz. We demonstrate differentiation of monomer and dimer forms of the GCN4-p1 leucine zipper, a coiled-coil structure well studied in molecular biology, and compare with the unstructured 33-residue monomer. GCN4-p1 is sequence segment associated with homodimerization of the transcription factor General Control Nonderepressible 4 (GCN4), which is involved in the control of amino acid synthesis in yeast. The differentiation between two oligomeric forms demonstrates the capabilities of improved solid-state nanopore platforms to extract structural information involving short peptide structures.

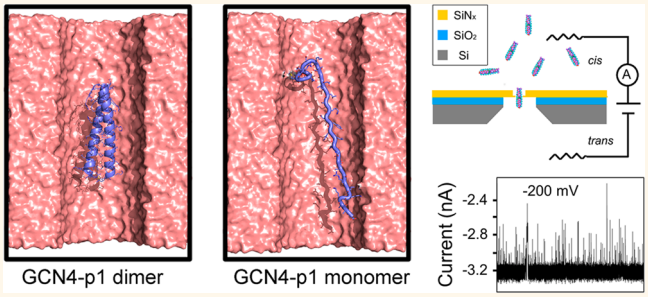

KEYWORDS: nanopore · GCN4 · single-molecule · leucine zipper · resistive-pulse

Nanopore sensors are promising platforms to realize highly sensitive, single-molecule detectors for the measurement of charged molecules.[1−4] A nanopore is a nanometer-sized hole in a thin membrane, which can be nonbiological such as silicon nitride (Figure 1A). Similar to cellular membrane porins in which molecules can translocate across the cell membrane, single molecules can be driven through a confined space one at a time through solid-state nanopores.[1−3,5] When an ionic solution is introduced on either side of a membrane containing a nanopore, ions and charged molecules can be electrophoretically driven through the nanopore and the ionic current measured and analyzed to extract information about the molecule. Distinction of molecules is made using both residence time (dwell-time) within the nanopore and the current amplitude signature or additional unique modulations (Figure 1B). Information, such as excluded volume,[2,6,7] charge,[8−10] hydrophobicity[6,11,12] and the chiral differences between enantiomeric amino acids, can be detected.[6,12,13] Since the sensing mechanism depends on the ionic current change, there is no need to label the molecule as in fluorescence microscopy, and salt concentrations can mimic those found under physiological conditions.

While much of the recent interest in nanopores has focused on DNA sequencing, the advantages of nanopore sensing extend to other molecules, such as polymers and proteins. Among the earliest molecules sensed was polyethylene glycol (PEG),[14−16] while sensing of protein molecules has been done mostly using small-diameter (<2 nm) protein nanopores (α-Hemolysin)[14,17,18] in bilayer membranes. Protein nanopores have obtained excellent results in the separation

* Address correspondence to drndic@physics.upenn.edu.

Received for review May 5, 2015 and accepted August 11, 2015.

Published online 10.1021/acsnano.5b02714

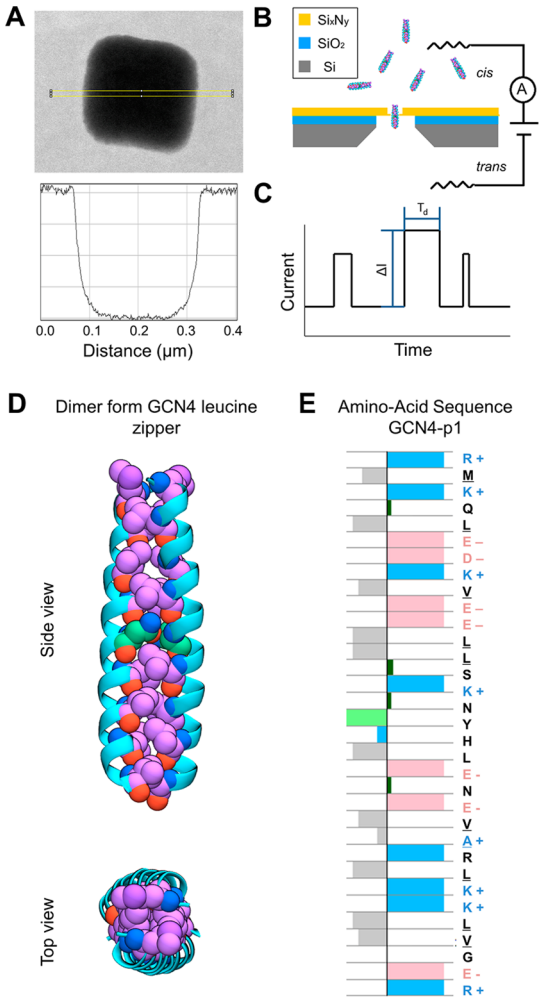

Figure 1. Nanopore setup and events. (A) TEM image of a typical thinned region of silicon nitride. The profile represents the intensity of a dark field (DF) TEM scan along the axis shown as a yellow rectangle. (B) Schematic of the nanopore setup. Nanopores are made in thin (<10 nm), freestanding silicon nitride suspended on 5 μm thick silicon oxide substrate. The positively charged GCN4-p1 protein is added to the *cis* (grounded) side of the membrane. Negative voltage is applied on the *trans* electrode, such that the positively charged GCN4-p1 molecules are driven through the nanopore. (C) Current fluctuations in the form of upward spikes are observed when GCN4-p1 enters into the nanopore interior. These spikes can be characterized by their current amplitude (ΔI) and dwell-time ($\Delta\tau$). (D) Schematic of the X-ray crystal structure of the GCN4-p1 segment used in this work. GCN4-p1 forms a polyleucine zipper with two GCN4-p1 segments forming a dimer. With addition of 3 M GdHCl, this structure denatures into monomers. (E) Amino acid sequence of the GCN4-p1 segment. Positively charged amino acids are shown in blue and labeled with a "+" sign. Negatively charged amino acids are shown in pink and labeled with a "-" sign. Hydrophilic residues are shown with boxes extending to the left and hydrophobic residues are shown with boxes extending to the right.

of small analytes. For example, Robertson *et al.* were able to separate poly(ethylene glycol) molecules differing less than 200 Da in molecular weight by using analysis of both blockade depth and mean residence times.[19] Additionally, protein nanopores have been used to study conformational changes in analyte proteins. Induced unfolding has been achieved by using several different mechanisms. Oukhaled *et al.* changed the unfolded state of the Maltose binding protein (MBP) by using different concentrations of chemical denaturant and observed changes in frequency and dwell-time of nanopore interaction events as a function of unfolding state.[20] Merstorf *et al.* used different concentrations of denaturants on the MBP and also a destabilized MBP mutant to observe changes in the unfolding transition of the wild type and the destabilized variant.[21] Similarly, Payet *et al.* used MBP mutants to observe the unfolding state by using elevated temperature.[22] Rodriguez-Larrea *et al.* used a DNA tethered protein to observe multistep unfolding of the thioredoxin using the electrical field of the nanopore.[23] While Pastoriza-Gallego *et al.* also used a tethered DNA−ligand chimera and with chemical denaturants to probe the unfolded state of the MBP mutant.[24]

One limitation of using protein nanopores is that their diameters are smaller than the size of many protein molecules in folded and functional forms. It is somewhat difficult to tailor the size of the pore, and the pore proteins must be correctly expressed, folded and positioned in membranes. Solid-state nanopores, however, have dimensions that can be readily tailored with close to subnanometer precision.[25,26] To date, solid-state nanopores have been used to detect proteins,[6,8,27−29] to detect the binding of proteins to nucleic acids,[3,7,25,30] to characterize size,[7,25,31] and to discriminate between large molecular weight proteins.[1,32] Previous nanopore studies have been able to resolve differences in molecular weight on the order of 100 kDa,[32] and herein, we have described how inorganic nanopores can be used to distinguish oligomerization states of single protein that differ by less than 10 kDa. Solid-state nanopores have also been used to probe unfolding mechanics and different conformation states of proteins. Studies have used chemical denaturants,[25,33] and the electric field generated by the nanopore,[3,34] and temperature[35] to induce structural changes the analytes studied. Detecting small molecules with such pores has proven difficult due to their short dwell times in the nanopore channel, which is often too short for significant detection with commercially available amplifiers.[36] Recent advances in both signal-to-noise and high bandwidth acquisition[6] have opened this field for study.[8,37]

In this paper, we demonstrate detection of proteins as small as 4 kDa, enabled by using a low noise amplifier (25pA$_{RMS}$ at 100 kHz)[6,12] combined with thin (<10 nm thick, 4−8 nm diameter) silicon nitride nanopores to maximize the signal levels by minimizing the nanopore thickness. We also demonstrate that silicon-based nanopores coupled with a recently developed, high performance amplifier[6,12] can be used to discriminate between the dimer and the denatured monomer

protein forms. Measurements were performed using GCN4-p1, a 33-amino acid polypeptide sequence from the General Control Nonderepressible 4 (GCN4) protein complex with hydrophobic repeats that forms a dimeric coiled-coil structure.[14] This protein system is biologically relevant because it is representative of the α-helical dimer (coiled coil) structure, a common structural motif found in transcription factors and intracellular receptors. The net charge of GCN4-p1 dimer is positive at neutral pH[14,17] and its structure is illustrated in Figure 1D. Because of its small size, the peptide dimer used here is also a useful model system to demonstrate a highly sensitive (both spatially and temporally) nanopore platform that is sensitive enough to analyze different structural features of small proteins. Specifically, we report a heterogeneous conformational structure of the protein within the nanopore, evidenced by a widespread in the protein-induced ionic current blockade amplitudes under normal salt conditions. Nonlinear voltage scaling of these current amplitude blockades was observed, with higher voltages producing a current blockade smaller than expected based on linear scaling. These observations indicate that the electric field in the nanopore interior partially denatures the GCN4-p1, splitting some dimers into monomer components. This is consistent with previous work demonstrating the partial denaturation of proteins under the influence of the electric field in a nanopore interior.[25] Additionally, by denaturing the dimer using guanidine hydrochloride (GdHCl) or elevated temperature, we show that the folded and denatured states exhibit distinct ionic current amplitude distributions. These observations illustrate the capabilities of new solid-state nanopore platforms to discriminate between the monomer and dimer forms of small proteins.

RESULTS AND DISCUSSION

In solution phase studies, the highly coiled dimer structure of GCN4-p1 was confirmed by circular dichroism (CD) spectra at room temperature at peptide concentrations of both 10 and 50 μM in 1 M NaCl and a 10 mM potassium phosphate buffer, pH 7.0. In solutions containing 3 M GdHCl, the CD spectra are consistent with the absence of helical secondary structure, consistent with a denatured monomer. Temperature dependent measurements were performed over the range of 21−95 °C, and indicate that GCN4-p1 denatures from the highly helical structure to an unstructured monomer at an estimated transition temperature of 54 °C

Nanopores with diameters between 4 and 8 nm were formed in silicon nitride membranes with thicknesses between 5 and 10 nm (Figure 1A) by a focused electron beam in a JEOL 2010F Transmission Electron Microscope (TEM). Translocation experiments were performed with solutions of 1 M NaCl and 50 mM potassium phosphate at pH 7.0, on both sides of the chamber (Figure 1B). The same solution conditions were used to confirm the secondary structure of the peptide GCN4-p1 using CD spectra as mentioned above. Open nanopore conductance ranged between 8 and 24 nS under these conditions. Only nanopores exhibiting stable (less than 400 pA RMS noise at 100 kHz) single-channel current signatures at voltages up to 500 mV were used. Twelve nanopores with less than 400 pA RMS at 100 kHz and that showed minimal expansion with time were selected out of a total of 59 nanopores tested GCN4-p1 was added to the *cis* (grounded, Figure 1B) side of the chamber at concentrations of 6, 10, or 35 μM. At positive applied voltages, no blockade in the single-channel current was observed for each concentration of the GCN4-p1, while at negative voltage polarity, multiple current blockade events were observed at each concentration. These observations are expected given a net positive charge of the GCN4-p1 dimer (+4e) under the given salt and pH conditions (Figure 1E).

Voltages of −100 to −500 mV, in increments of −100 mV, were applied across the nanopore. Current was measured with a VC100 [Chimera Instruments, New York, NY] high-bandwidth, low-noise voltage-clamp amplifier and digitally filtered with a fourth-order Bessel low-pass filter at 100 kHz. This amplifier was previously used in DNA and protein translocation measurements.[6,8] Event blockades were characterized by the event duration (dwell-time, τ_d) and event amplitude (ΔI). Event amplitudes are expected to scale linearly with both applied voltage and the excluded volume of the measured molecule.[3,7,25] A rough estimate can be given by the formula,

$$\Delta I/V \cong \frac{\pi X}{6\rho L^2} \quad (1)$$

where V is the applied potential, X is the excluded volume of the molecule, ρ is the ionic solution resistivity, and L is the effective pore thickness.[7,25,31] This above model does not take into account the adsorption of screening counterions to the GCN4-p1 molecule, which has been shown to be important to blockade depth in both DNA[38] and polymers.[39] A full account of the absorption of counterions to GCN4-p1 would likely require a full molecular dynamics treatment that was beyond the scale of our work here.

Figure 2A shows a scatter plot of $\Delta I/V$ *vs* τ_d at the given voltages. According to eq 1, $\Delta I/V$ should remain constant if the excluded volume of the protein remains the same under applied voltages. However, different distributions were observed for $\Delta I/V$ under different applied voltages. $\Delta I/V$ shows a clustering of lower amplitude current blockades (<1 nA/V) and, additionally, a range of larger amplitude $\Delta I/V$ (up to 5 nA/V) that show up at the upper left corner of the scatterplot. These larger amplitude $\Delta I/V$ events are more prominent for

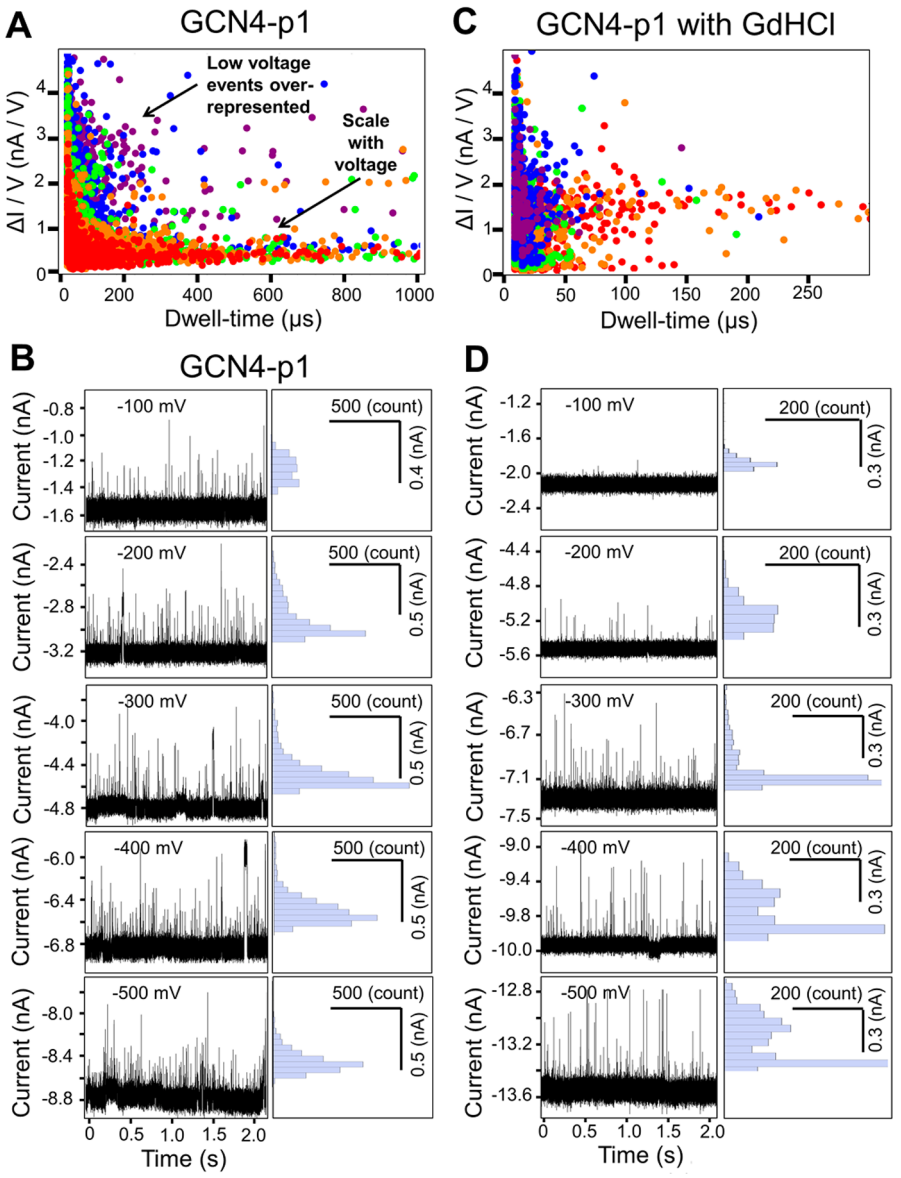

Figure 2. Representative GCN4-p1 induced current blockade events in 1 M NaCl, 50 mM potassium phosphate, pH 7.0. Nanopore was 7 nm in diameter and <10 nm thick. GCN4-p1 concentration was 6 μM. (A) Scatterplot of current blockade events with blockade amplitude normalized to the open pore current. Applied voltages were −100 mV (purple), −200 mV (blue), −300 mV (green), −400 mV (orange), and −500 mV (red). Note that lower amplitude event amplitudes overlap, showing expected voltage scaling, whereas events induced at lower voltages are over-represented for the larger ($\Delta I/V$) events. (B) Representative traces for 1 M NaCl, 50 mM potassium phosphate at voltages of −100, −200, −300, −400, and −500 mV. Event amplitude histograms are shown aligned next to the current traces. Note the large tail of higher-amplitude events seen below −200 mV that become less prominent as voltage increases. (C) GCN4-p1 induced current blockade events in 1 M NaCl, 50 mM potassium phosphate with 3 M GdHCl added to the *cis* side of the chamber (same pore). Scatterplot of current blockade events with blockade amplitude normalized to the open pore current. Applied voltages were −100 mV (purple), −200 mV (blue), −300 mV (green), −400 mV (orange), and −500 mV (red). Note that ($\Delta I/V$) event amplitudes overlap, showing expected voltage scaling. (D) Representative traces with 3 M GdHCl added to the *cis* side of the chamber at voltages of −100, −200, −300, −400, and −500 mV. Event amplitude histograms are shown aligned next to the current traces. Event amplitude histograms show a maximum amplitude peak that scales with increased voltage and, at higher voltages, a shallow amplitude blockade peak with a large number of events. This second shallow peak is hidden within the baseline current noise for voltages with magnitude less than −300 mV.

lower applied voltages (100 mV), than for higher applied voltages (>300 mV).

A possible explanation for the absence of larger amplitude $\Delta I/V$ events at higher voltages is a voltage-induced denaturation of the GCN4-p1 dimer into its monomer peptides. This is likely due to the heterogeneous charge structure of the GCN4-p1 amino acid sequence (Figure 1D). Solid-state nanopore induced protein denaturation has been studied elsewhere,[3,25,40,41] and could explain the shift away from larger amplitude (ΔI) events at high voltages. In particular, dimers have a larger excluded volume within the pore than monomers. Therefore, by eq 1, dimers will give a larger current blockade than monomers.

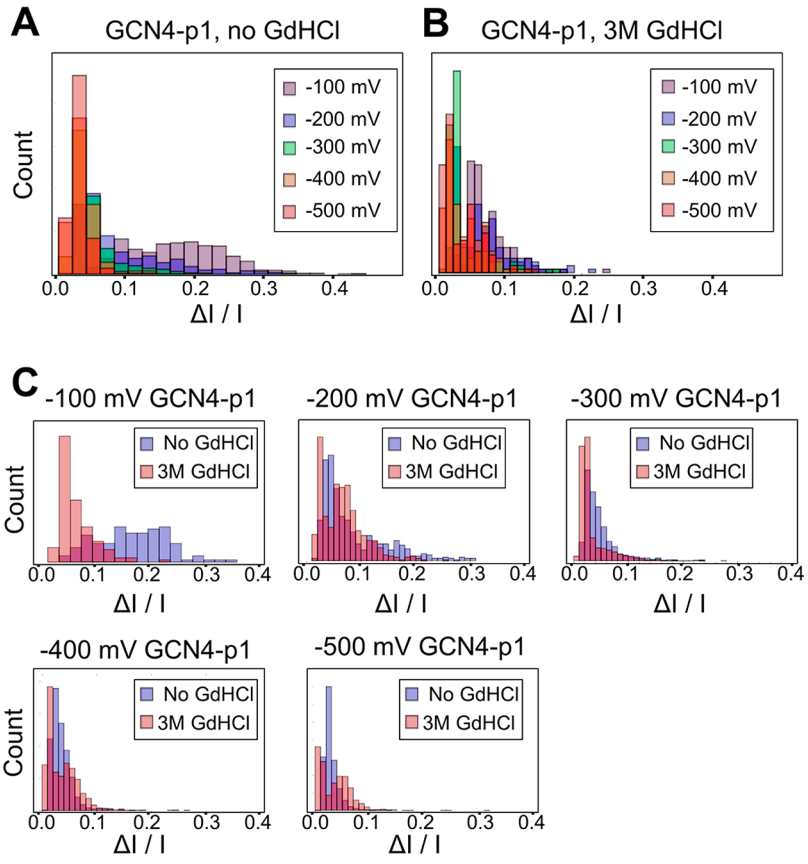

Figure 3. Comparison of current blockade amplitude (Δ*I*) histograms for GCN4-p1 events in the same 7 nm diameter nanopore both with and without 3 M GdHCl on the *cis* side of the chamber. Solution was 1 M NaCl, 50 mM potassium phosphate, pH 7.0. (A) Normalized current blockade amplitudes (Δ*I*/*I*) without GdHCl. The count has been normalized so that each voltage has the same number of events. Lower magnitude voltages display events with much larger Δ*I*/*I* than higher magnitude voltages. (B) Normalized current blockade amplitudes (Δ*I*/*I*) with 3 M GdHCl, 1 M NaCl, 50 mM potassium phosphate in the *cis* chamber. The count has been normalized so that each voltage has the same number of events. (Δ*I*/*I*) peaks overlap for the measured voltages. (C) Direct comparison of normalized current amplitude blockades (Δ*I*/*I*) for nanopores with and without GdHCl solution. Voltage of −100 mV shows a clear separation of current blockade amplitudes, with GdHCl-free solution having larger normalized current amplitude events. At −200 mV, a tail of large amplitude events still exists for GdHCl solution.

We caution that more sophisticated simulations would be required to confirm this hypothesis.

Experiments using a solution containing 3 M guanidine hydrochloride (GdHCl), 1 M NaCl, and 50 mM potassium phosphate at pH 7.0 were performed immediately after measurements on GCN4-p1. GCN4-p1 concentrations were matched to be the same as those in the absence of GdHCl (6, 10, or 35 μM). The bulk conductivity of 3 M GdHCl containing solution was higher than that containing 1 M NaCl alone by a factor of 3.4 ± 0.5 (no GdHCL/GdHCl). Solution in the *trans* chamber remained at 1 M NaCl. The measured conductance across the nanopore increased by 1.4 ± 0.2 times with a switch to 3 M GdHCl, 1 M NaCl, and 50 mM potassium phosphate at pH 7.0 in the *cis* chamber. This is in agreement with a half−half solution mixing within the interior of the nanopore of the solutions from both sides. Previous studies showed similar trends in nanopore conductance with asymmetric solutions.[2,42] Control experiments measuring the CD spectra of GCN4-p1 indicate that the protein is denatured (no helical secondary structure) in 3 M GdHCl.

Figure 2B shows a scatter plot of Δ*I*/*V* for GCN4-p1 with 3 M GdHCl added. The scatter of Δ*I*/*V* overlaps for the applied voltages, suggesting that the excluded volume of the denatured monomer GCN4-p1 remains constant under the different applied voltages.

The different events scaling with applied voltage is shown in Figure 2C, which shows representative events for GCN4-p1 without GdHCl, and Figure 2D, which shows representative events for GCN4-p1 with 3 M GdHCl added.

To compare event amplitudes (Δ*I*) before and after addition of 3 M GdHCl, we normalized to the open pore current (*I*), which provided a normalized ratio of Δ*I*/*I*. To control for possible nanopore expansion with time, the open pore current (*I*) in GdHCl experiments was fixed to the value $I = 1.4I_{initial}$, where $I_{initial}$ was the baseline current in the non-GdHCl containing solution. This corresponds to the initial conductivity increase measured with the first introduction of GdHCl. This procedure avoids underestimation of the ratio Δ*I*/*I* that can arise from pore enlargement, which increases the

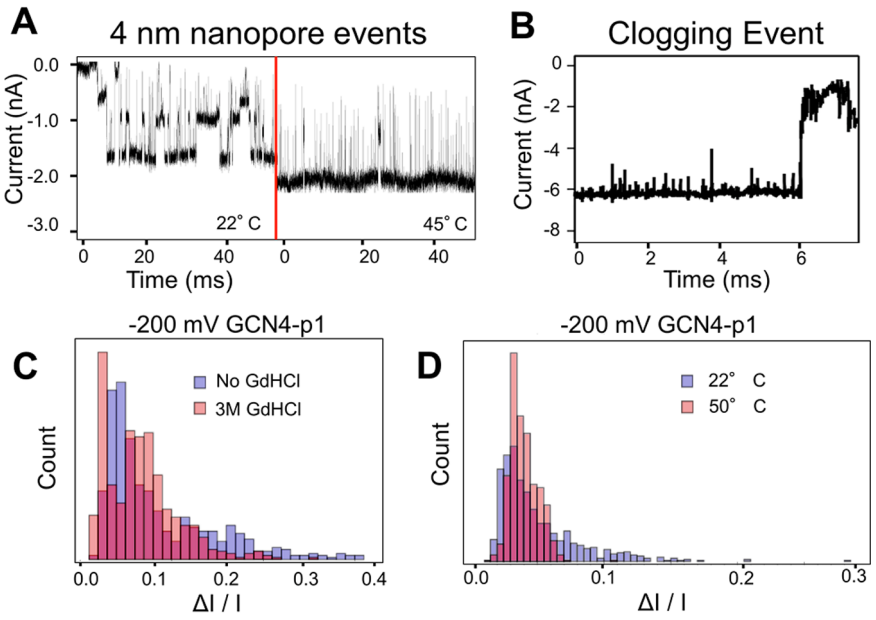

Figure 4. GCN4-p1 translocation events at raised temperatures. (A) GCN4-p1 induced events measured with a 4 nm diameter nanopore. Note the appearance of long-lived (>5 ms) half-amplitude events at room temperature. Larger scale events cause current blockades to near 0 nA. After the temperature of solution was increased to 45 °C, events transitioned to shorter dwell-times and the largest amplitude events no longer dropped to 0 nA. Solution was 1 M NaCl, 50 mM potassium phosphate buffer, pH 7.0. Applied voltage was −200 mV. (B) An example of a clogging event in a 6 nm diameter nanopore at 52 °C. (C) Comparison of normalized current blockade amplitude histograms. The first shows the difference in normalized current blockades with and without 3 M GdHCl at an applied voltage of −200 mV. Data set taken with a 7 nm diameter nanopore. The second shows the difference in normalized current blockades at room temperature and at 50 °C. Dark red is the overlap of the two histograms. Data set taken with a 6 nm diameter nanopore.

current *I*. Figure 3A shows normalized $\Delta I/I$ for GCN4-p1 without GdHCl and Figure 3B shows normalized $\Delta I/I$ for GCN4 with 3 M GdHCl added.

We posit that the excluded volume for a monomer denatured by voltage should be comparable to the excluded volume for a monomer denatured by GdHCl. The amplitude of ΔI will be proportional to the excluded volume of a monomer. Therefore, if voltage has denatured the GCN4 into a monomer, the $\Delta I/I$ should look the same with and without GdHCl. Figure 3C shows a comparison of the distributions of $\Delta I/I$ for different applied voltages both with and without GdHCl added to solution. The distributions of $\Delta I/I$ in the presence and absence of GdHCl are similar at high voltages (>400 mV) but differ at low voltages (100 mV). Therefore, we infer that high voltages (>400 mV) lead to denaturation of the GCN4-p1 into a monomer, and at low voltages (100 mV), the dimeric form is maintained. In future experiments it may be possible to distinguish between dimer, trimer, and tetramer forming variants of the GCN4 Leucine Zipper and other peptide oligomers or to quantify the relative populations of the dimer and monomer forms of small proteins such as GCN4-p1.

GCN4-p1 at Higher Temperatures. To further compare the dimer to denatured monomers of GCN4-p1, temperature dependent measurements were performed. The GCN4-p1 denatures from a dimer to an unstructured monomer at high temperature, consistent with measured CD spectra, where the transition temperature (estimated here as the maximum in the slope of the molar ellipticity at 222 nm as a function of the temperature) of GCN4-p1 in 1 M NaCl was measured to be T_m = 54 °C.

Figure 4A shows measurements of 35 μM GCN4-p1 added to a system containing a 4 nm diameter pore between the two chambers. Events are interspersed between 0 nA and the baseline current (−1.6 nA), with many long-lived, half-amplitude (−0.9 nA) events. We interpret that the more complex distribution of events (Figure 4A) at the lower temperature is due to the increased entropic barrier created by the smaller pore, which is near the same linear dimension as the GCN4-p1 dimers.[2,43−45] At the higher temperature (and higher voltages), GCN4-p1 is largely monomeric and unstructured, facilitating the translocation of the peptide.[2,7,43] (Figure 4A). Note that no current blockades were observed to reach 0 nA at the higher temperature (45 °C).

Long-lived "adsorption" current blockades that did not revert to the original baseline current, presumably due to clogging of the pore (Figure 4B), were observed while raising the temperature during these experiments. We interpret these blockades as a temperature-based unfolding of the GCN4-p1 dimer into its monomer form.[9,10,22,25,44,46] Temperature-based unfolding will expose hydrophobic leucines. Similar hydrophobic exposure has been shown to drive adsorption of protein

molecules onto silicon−nitride membranes.[11,47,48] Analysis of events at high temperature was complicated by the high rate of adsorption events, which limited the amount of data taken before irreversible pore fouling. The comparison of normalized low temperature (22 °C) events to events at 50 °C is given in Figure 4C. Interestingly, the larger tail in the distribution of events for $\Delta I/I > 0.6$ disappears at the higher temperature, suggesting that dimers are no longer in solution.

CONCLUSIONS

In summary, we demonstrate detection of small peptides with lengths as short as 33 amino acids and molecular weights as low as 4 kDa with sub-10 nm thick solid-state nanopores and a low-noise amplifier. Translocation measurements of GCN4-p1 peptide leucine zipper molecules showed that ionic current amplitude scales nonlinearly with voltage, suggesting a voltage-induced unfolding of the GCN4-p1 leucine zipper into its monomer components. At lower voltages, events having large-amplitudes of $\Delta I/V$ were more prevalent and we assign these to the dimer form of GCN4-p1. We attribute smaller amplitude ($\Delta I/V < 2$ nA/V) events to the GCN4-p1 monomer domain and note that these events scaled linearly with applied voltage. The main evidence for the dimer is the presence of events at large $\Delta I/V$. Both chemically induced denaturation using 3 M GdHCl and also temperature-induced denaturation were used as controls. For GdHCl-denatured monomeric GCN4-p1, the major amplitude distribution peak in $\Delta I/V$ scaled linearly with applied voltage. We were able to distinguish the dimers and monomers by comparing normalized current blockade histograms of GCN4-p1 with and without GdHCl in solution. Temperature denaturation of the GCN4-p1 peptide induced long-lived adsorption events onto the nanopore interior, which we attribute to the exposure of the hydrophobic interior leucines. Extraction of non-adsorption data (events with dwell-times less than 500 ms) at high temperature showed event peaks that were smaller in normalized blockade amplitude than the large-scale dimer-events at room temperature. We attribute this change in amplitudes to the difference in oligomerization state at the different temperatures; events at high temperatures result from translocating monomers, which are the predominant form of the protein due to thermal (and voltage) denaturation. At higher temperature, denaturation occurs at lower voltages due to the reduction of the energetic penalty to unravel the dimer *via* voltage.

Finally, we show how voltage-induced denaturation of peptides presents a challenge for stochastic sensing of proteins using nanopores: application of lower voltages reduces the probability of protein denaturation, but it also decreases signal-to-noise ratio. Future experiments should therefore make use of recent developments in lower noise nanopore chips to attempt detection of proteins at lower voltages with sufficiently high signal-to-noise ratios.[13,49]

METHODS

Nanopore Fabrication. Nanopores were formed in ultrathin, freestanding films of low-stress silicon nitride (SiN_x) using a 2010F JEOL Transmission Electron Microscope (TEM), as described previously.[6,15] The SiN_x was grown by Low Pressure Chemical Vapor Deposition (LPCVD) on 5 μm of silicon oxide (SiO_2) on a standard p-doped silicon wafer. The 5×5 mm^2 chips of silicon were patterned using standard optical lithography and the center of the chip was back etched using 40% potassium hydroxide (KOH) to create a 20×20 μm^2 freestanding window of SiO_2 and SiN_x. SiO_2 was removed by a buffered oxide etch (BOE) to leave a 50 nm thick freestanding SiN_x membrane. Further thinning of the membrane was performed by first patterning smaller areas (100×100 nm^2) using electron beam lithography and then etching them using CHF3 plasma.[2,49]

Nanopore diameters were measured using bright-field TEM (Figure 1A). The thickness measurements were assessed by using mass contrast made from dark-field TEM, as shown in Figure 1A.[6,26]

Peptide Synthesis. The peptide GCN4-p1 was synthesized (100 μmol scale) by solid phase peptide synthesis, using 9-fluorenylmethoxycarbonyl (FMOC) chemistry, on a Liberty1 Automated Microwave Peptide Synthesizer (CEM, Matthews, NC). Additional information is given in the Supporting Information.

Purification. Peptides were purified >95% using high-performance liquid chromatography (HPLC). A binary gradient between (A) 0.1% trifluoroacetic acid (TFA) in water and (B) 90% acetonitrile, 9.9% water, and 0.1% TFA was used. Peptide GCN4-p1 was purified using a Vydac C18 column 30×250 cm, 300 Å pore size, 10 mm particle size (Grace, Columbia, MD). Elution was carried out using a two-step gradient: step 1, 20% B to 35% B over 5 min; step 2, 35% B to 55% B over 20 min. A flow-rate of 42 mL/min was used for both steps. The mass of the purified peptide was confirmed by MALDI-MS using a Bruker Ultraflex III MALDI-TOF/TOF (Bruker Daltonics, Billerica, MA). A mass of 4036.112 *m/z* was observed (expected, 4037.673 avg., 4035.194 monoisotopic).

CD Spectroscopy. CD spectroscopy was performed on peptide GCN4-p1 using an AVIV Model 410 Circular Dichroism Spectrophotometer (AVIV Biomedical, Lakewood, NJ). The concentrations of the peptide stock solution 50 μM was determined using UV absorbance at 280 nm, (ε = 1330), and diluted to the appropriate concentration in buffer. Wavelength scans were run at 21 °C, starting from 260 to −200 nm with a 1 nm step size and 15 s averaging time. Temperature dependent measurements, monitoring 222 nm (15 s averaging time), were performed from 4 to 96 °C with a 1 min equilibration time between temperature steps and a 5 min wait time prior to the reverse scans. The wavelength scans with 3 M GdHCl were performed using the identical conditions at 25 °C.

Nanopore Measurements. The nanopore chip was cleaned in a heated piranha solution followed by thorough rinsing with distilled H_2O, and was then placed in a fluoropolymer cell using a quick-cure silicon elastomer.[12,27−29]

After it was sealed into the cell, a solution of 1 M NaCl and 50 mM potassium phosphate at pH 7.0 was introduced onto both sides of the nanopore chip and Ag/AgCl electrodes were placed in contact with the solution. We define the *cis* side of the chamber as the side in contact with the reference (grounded) electrode and the *trans* side as the side in contact with the voltage-bearing electrode.

Current measurements were made by applying a voltage bias across the nanopore and measuring the resulting current

by using a VC100 high-bandwidth, low-noise voltage-clamp amplifier (Chimera Instruments, New York, NY). The amplifier is capable of high bandwidth acquisition: it includes a fourth-order Bessel low-pass filter at 1 MHz, and signals are digitized at 4−6 MS/s. Experiments proceeded only if the nanopore exhibited a stable baseline ionic current and conductance that was in agreement with that expected from the equation

$$I = V([\mu_{Na^+} + \mu_{Cl^-}]n_{NaCl}e)\left(\frac{4h_{eff}}{\pi d^2} + \frac{1}{d}\right)^{-1} \quad (2)$$

where I is the open-state current of the nanopore and V is the applied transmembrane voltage.[30,50] Here, μ_{Na^+} and μ_{Cl^-} are the electrophoretic mobilites of the Na^+ ions and Cl^- ions, respectively; e, h_{eff}, and d denote the elementary charge, the effective thickness of the nanopore, and its diameter, respectively, and n_{NaCl} is the number density for Na and Cl. Nanopores deviating from the expected conductance by more than 30% were not used.

Nanopore thickness was estimated from the ratio of the dark-field intensity in a TEM image between the thinned and unthinned potion of the membrane. The estimate of 10 nm was made by observing the intensity ratio between these regions was 1/5, and the starting nitride thickness was 50 nm.[7,12]

A concentrated solution of GCN4-p1 was added to the *cis* (grounded) side of the chamber and mixed by pipetting up and down several times. Final solution concentrations were 6, 10, or 35 μM. A negative voltage bias was applied, which resulted in GCN4-p1 induced events and current *vs* time measurements were taken. Controls were checked at positive bias to ensure no event signals were present.

Comparison experiments were made with 3 M GdHCl, 1 M NaCl, and 50 mM potassium phosphate immediately after completing measurements on the GCN4-p1 sample. For GdHCl and GCN4-p1 measurements, an aliquot of the solution was made by premixing outside of the chamber to the desired concentration of either 6, 10, or 35 μM, and set for several minutes to allow time for the protein to denature. The *cis* side of the chamber was flushed with 1 M NaCl and 50 mM potassium phosphate and then completely evacuated. The GdHCl, GCN4-p1 solution was immediately added to the *cis* chamber. Conductance was checked to ensure proper levels (expected conductance increase was 1.4 times the 1 M NaCl baseline due to increased conductivity of the GdHCl) and negative bias potentials were applied as before.

Temperature control experiments were preformed after measurement on the GCN4-p1 at room temperature. The translocation measurement setup features a temperature regulation system using a thermoelectric device connected to a copper block that houses the cell. Temperature was measured by direct immersion of the thermometer into the *cis* side solution and the chamber was sealed with silicon elastomer to prevent evaporation. The thermoelectric device was turned off during current measurements to reduce system noise.

Data Acquisition and Analysis. Initial ionic current data was acquired at 4−6 MS/s sampling with a fourth-order Bessel low-pass filter at 1 MHz. The data was partitioned in 1.6-s intervals using Matlab (MathWorks, Natick, MA). Postacquisition analysis was performed using the open source nanopore translocation analysis software PyPore (http://parkin.github.io/pypore/) developed by Drndić lab. Data was digitally filtered to (4-pole Bessel) 100 kHz and event traces were scanned for upward translocation events. Events were registered *via* a 5-sigma search from the open current baseline level.

Due to high adsorption rates at high temperature, traces were manually searched at 50 °C to extract only events within nonclogged part of the current trace. During high temperature (>40 °C) measurements, reversal of bias potential was often able to dislodge clogged molecules and return the nanopore to its preclog conductance. In that case, current measurements were continued until the next clogging event occurred. All events were collated later and exported to Mathematica 8.0 (Wolfram Research, Inc., Champaign, IL) for analysis.

Methods of Correcting Amplitudes during Analysis. Due to the increase in conductivity of the 3 M GdHCl solutions, normalization of current amplitude spikes was needed to compare events. This was achieved by multiplying the current event values in the GdHCl samples by 1.4. This number represents the change in conductance of the nanopore when GdHCl solution is introduced on the *cis* side of the chamber (conductance increases). This was done rather than just the ratio of the signal to open pore current to eliminate any discrepancies that might be introduced by pore enlargement with time. Measured conductance of 1 M NaCl *vs* 3 M GdHCl was 1.4 ± 0.2, in good agreement with the expected change if there is 50% mixing in the pore interior.

Conflict of Interest: The authors declare no competing financial interest.

Supporting Information Available: The Supporting Information is available free of charge on the ACS Publications website at DOI: 10.1021/acsnano.5b02714.

CD measurements, dwell-time of GCN4-p1 events, interevent time of GCN4-p1 events, current traces at different GCN4-p1 concentrations and at different temperatures, search parameters for clogging events, and control traces at positive voltage polarity (PDF)

Acknowledgment. The authors thank W. Parkin for creating the PyPore analysis software and his assistance with analysis and Wenhao Liu for help with figures. This work was supported by the Nano/Bio Interface Center through the National Science Foundation NSEC DMR08-32802 and by the NIH Grants R21HG004767 and R01HG006879. We gratefully acknowledge NSF-MRSEC DMR-1120901 for TEM electron microscopy facility and other infrastructural resources.

REFERENCES AND NOTES

1. Plesa, C.; Kowalczyk, S. W.; Zinsmeester, R.; Grosberg, A. Y.; Rabin, Y.; Dekker, C. Fast Translocation of Proteins Through Solid State Nanopores. *Nano Lett.* **2013**, *13*, 658–663.
2. Movileanu, L. *Single-Molecule Detection of Proteins Using Nanopores*; Barth, F., Humphrey, J., Srinivasan, M., Eds.; Springer Wien: New York, 2014; pp 1−20.
3. Talaga, D. S.; Li, J. Single-Molecule Protein Unfolding in Solid State Nanopores. *J. Am. Chem. Soc.* **2009**, *131*, 9287–9297.
4. Reiner, J. E.; Balijepalli, A.; Robertson, J. W. F.; Campbell, J.; Suehle, J.; Kasianowicz, J. J. Disease Detection and Management *via* Single Nanopore-Based Sensors. *Chem. Rev.* **2012**, *112*, 6431–6451.
5. Kasianowicz, J. J.; Brandin, E.; Branton, D.; Deamer, D. W. Characterization of Individual Polynucleotide Molecules Using a Membrane Channel. *Proc. Natl. Acad. Sci. U. S. A.* **1996**, *93*, 13770–13773.
6. Venta, K.; Shemer, G.; Puster, M.; Rodríguez-Manzo, J. A.; Balan, A.; Rosenstein, J. K.; Shepard, K.; Drndić, M. Differentiation of Short, Single-Stranded DNA Homopolymers in Solid-State Nanopores. *ACS Nano* **2013**, *7*, 4629–4636.
7. Ledden, B.; Fologea, D.; Talaga, D. S.; Li, J. *Sensing Single Protein Molecules with Solid-State Nanopores*; Springer: Boston, MA, 2011; pp 129−150.
8. Larkin, J.; Henley, R. Y.; Muthukumar, M.; Rosenstein, J. K.; Wanunu, M. High-Bandwidth Protein Analysis Using Solid-State Nanopores. *Biophys. J.* **2014**, *106*, 696–704.
9. Stefureac, R.; Long, Y.-T.; Kraatz, H.-B.; Howard, P.; Lee, J. S. Transport of Alpha-Helical Peptides Through Alpha-Hemolysin and Aerolysin Pores. *Biochemistry* **2006**, *45*, 9172–9179.
10. Katkar, H. H.; Muthukumar, M. Effect of Charge Patterns Along a Solid-State Nanopore on Polyelectrolyte Translocation. *J. Chem. Phys.* **2014**, *140*, 135102.
11. Mohammad, M. M.; Prakash, S.; Matouschek, A.; Movileanu, L. Controlling a Single Protein in a Nanopore Through Electrostatic Traps. *J. Am. Chem. Soc.* **2008**, *130*, 4081–4088.
12. Wanunu, M.; Bhattacharya, S.; Xie, Y.; Tor, Y.; Aksimentiev, A.; Drndic, M. Nanopore Analysis of Individual RNA/Antibiotic Complexes. *ACS Nano* **2011**, *5*, 9345–9353.

13. Boersma, A. J.; Bayley, H. Continuous Stochastic Detection of Amino Acid Enantiomers with a Protein Nanopore. *Angew. Chem., Int. Ed.* **2012**, *51*, 9606–9609.
14. O'Shea, E. K.; Klemm, J. D.; Kim, P. S.; Alber, T. X-Ray Structure of the GCN4 Leucine Zipper, a Two-Stranded, Parallel Coiled Coil. *Science* **1991**, *254*, 539–544.
15. Bezrukov, S. M.; Vodyanoy, I.; Parsegian, V. A. Counting Polymers Moving Through a Single Ion Channel. *Nature* **1994**, *370*, 279–281.
16. Krasilnikov, O. V.; Sabirov, R. Z.; Ternovsky, V. I.; Merzliak, P. G.; Muratkhodjaev, J. N. A Simple Method for the Determination of the Pore Radius of Ion Channels in Planar Lipid Bilayer Membranes. *FEMS Microbiol. Lett.* **1992**, *5*, 93–100.
17. Harbury, P. B.; Zhang, T.; Kim, P. S.; Alber, T. A Switch Between Two-, Three-, and Four-Stranded Coiled Coils in GCN4 Leucine Zipper Mutants. *Science* **1993**, *262*, 1401–1407.
18. Song, L.; Hobaugh, M. R.; Shustak, C.; Cheley, S.; Bayley, H.; Gouaux, J. E. Structure of Staphylococcal A-Hemolysin, a Heptameric Transmembrane Pore. *Science* **1996**, *274*, 1859–1865.
19. Robertson, J. W. F.; Rodrigues, C. G.; Stanford, V. M.; Rubinson, K. A.; Krasilnikov, O. V.; Kasianowicz, J. J. Single-Molecule Mass Spectrometry in Solution Using a Solitary Nanopore. *Proc. Natl. Acad. Sci. U. S. A.* **2007**, *104*, 8207–8211.
20. Oukhaled, G.; Mathé, J.; Biance, A.-L.; Bacri, L.; Betton, J.-M.; Lairez, D.; Pelta, J.; Auvray, L. Unfolding of Proteins and Long Transient Conformations Detected by Single Nanopore Recording. *Phys. Rev. Lett.* **2007**, *98*, 158101.
21. Merstorf, C.; Cressiot, B.; Pastoriza-Gallego, M.; Oukhaled, A.; Betton, J.-M.; Auvray, L.; Pelta, J. Wild Type, Mutant Protein Unfolding and Phase Transition Detected by Single-Nanopore Recording. *ACS Chem. Biol.* **2012**, *7*, 652–658.
22. Payet, L.; Martinho, M.; Pastoriza-Gallego, M.; Betton, J.-M.; Auvray, L.; Pelta, J.; Mathé, J. Thermal Unfolding of Proteins Probed at the Single Molecule Level Using Nanopores. *Anal. Chem.* **2012**, *84*, 4071–4076.
23. Rodriguez-Larrea, D.; Bayley, H. Multistep Protein Unfolding During Nanopore Translocation. *Nat. Nanotechnol.* **2013**, *8*, 288–295.
24. Pastoriza-Gallego, M.; Breton, M.-F.; Discala, F.; Auvray, L.; Betton, J.-M.; Pelta, J. Evidence of Unfolded Protein Translocation Through a Protein Nanopore. *ACS Nano* **2014**, *8*, 11350–11360.
25. Li, J.; Fologea, D.; Rollings, R.; Ledden, B. Characterization of Protein Unfolding with Solid-State Nanopores. *Protein Pept. Lett.* **2014**, *21*, 256–265.
26. Storm, A. J.; Chen, J. H.; Ling, X. S.; Zandbergen, H. W.; Dekker, C. Fabrication of Solid-State Nanopores with Single-Nanometre Precision. *Nat. Mater.* **2003**, *2*, 537–540.
27. Firnkes, M.; Pedone, D.; Knezevic, J.; Döblinger, M.; Rant, U. Electrically Facilitated Translocations of Proteins Through Silicon Nitride Nanopores: Conjoint and Competitive Action of Diffusion, Electrophoresis, and Electroosmosis. *Nano Lett.* **2010**, *10*, 2162–2167.
28. Han, A.; Creus, M.; Schürmann, G.; Linder, V.; Ward, T. R.; de Rooij, N. F.; Staufer, U. Label-Free Detection of Single Protein Molecules and Protein-Protein Interactions Using Synthetic Nanopores. *Anal. Chem.* **2008**, *80*, 4651–4658.
29. Li, J.; Golovchenko, J. A. Solid-State Nanopore for Detecting Individual Biopolymers. *Methods Mol. Biol.* **2009**, *544*, 81–93.
30. Smeets, R. M. M.; Kowalczyk, S. W.; Hall, A. R.; Dekker, N. H.; Dekker, C. Translocation of RecA-Coated Double-Stranded DNA Through Solid-State Nanopores. *Nano Lett.* **2009**, *9*, 3089–3095.
31. DeBlois, R. W. Counting and Sizing of Submicron Particles by the Resistive Pulse Technique. *Rev. Sci. Instrum.* **1970**, *41*, 909.
32. Fologea, D.; Ledden, B.; McNabb, D. S.; Li, J. Electrical Characterization of Protein Molecules by a Solid-State Nanopore. *Appl. Phys. Lett.* **2007**, *91*, 053901.
33. Oukhaled, A.; Cressiot, B.; Bacri, L.; Pastoriza-Gallego, M.; Betton, J.-M.; Bourhis, E.; Jede, R.; Gierak, J.; Auvray, L.; Pelta, J. Dynamics of Completely Unfolded and Native Proteins Through Solid-State Nanopores as a Function of Electric Driving Force. *ACS Nano* **2011**, *5*, 3628–3638.
34. Freedman, K. J.; Haq, S. R.; Edel, J. B.; Jemth, P.; Kim, M. J. Single Molecule Unfolding and Stretching of Protein Domains Inside a Solid-State Nanopore by Electric Field. *Sci. Rep.* **2013**, *3*, 1638.
35. Freedman, K. J.; Jürgens, M.; Prabhu, A.; Ahn, C. W.; Jemth, P.; Edel, J. B.; Kim, M. J. Chemical, Thermal, and Electric Field Induced Unfolding of Single Protein Molecules Studied Using Nanopores. *Anal. Chem.* **2011**, *83*, 5137–5144.
36. Kasianowicz, J. J.; Robertson, J. W. F.; Chan, E. R.; Reiner, J. E.; Stanford, V. M. Nanoscopic Porous Sensors. *Annu. Rev. Anal. Chem.* **2008**, *1*, 737–766.
37. Nir, I.; Huttner, D.; Meller, A. Direct Sensing and Discrimination Among Ubiquitin and Ubiquitin Chains Using Solid-State Nanopores. *Biophys. J.* **2015**, *108*, 2340–2349.
38. Kesselheim, S.; Müller, W.; Holm, C. Origin of Current Blockades in Nanopore Translocation Experiments. *Phys. Rev. Lett.* **2014**, *112*, 018101.
39. Reiner, J. E.; Kasianowicz, J. J.; Nablo, B. J.; Robertson, J. W. F. Theory for Polymer Analysis Using Nanopore-Based Single-Molecule Mass Spectrometry. *Proc. Natl. Acad. Sci. U. S. A.* **2010**, *107*, 12080–12085.
40. Pastoriza-Gallego, M.; Gibrat, G.; Thiebot, B.; Betton, J.-M.; Pelta, J. Biochimica Et Biophysica Acta. *Biochim. Biophys. Acta, Biomembr.* **2009**, *1788*, 1377–1386.
41. Cressiot, B.; Oukhaled, A.; Patriarche, G.; Pastoriza-Gallego, M.; Betton, J.-M.; Auvray, L.; Muthukumar, M.; Bacri, L.; Pelta, J. Protein Transport Through a Narrow Solid-State Nanopore at High Voltage: Experiments and Theory. *ACS Nano* **2012**, *6*, 6236–6243.
42. Wanunu, M.; Morrison, W.; Rabin, Y.; Grosberg, A. Y.; Meller, A. Electrostatic Focusing of Unlabelled DNA Into Nanoscale Pores Using a Salt Gradient. *Nat. Nanotechnol.* **2010**, *5*, 160–165.
43. Dudko, O. K.; Mathé, J.; Szabo, A.; Meller, A.; Hummer, G. Extracting Kinetics From Single-Molecule Force Spectroscopy: Nanopore Unzipping of DNA Hairpins. *Biophys. J.* **2007**, *92*, 4188–4195.
44. Kasianowicz, J. J. Bio-Inspired Nanopore-Based Sensors. comment on "Nanopores: a Journey Towards DNA Sequencing" by M. Wanunu. *Phys. Life Rev.* **2012**, *9*, 170–171.
45. Dudko, O. K.; Hummer, G.; Szabo, A. Intrinsic Rates and Activation Free Energies From Single-Molecule Pulling Experiments. *Phys. Rev. Lett.* **2006**, *96*, 108101.
46. Mohammad, M. M.; Movileanu, L. Excursion of a Single Polypeptide Into a Protein Pore: Simple Physics, but Complicated Biology. *Eur. Biophys. J.* **2008**, *37*, 913–925.
47. Niedzwiecki, D. J.; Grazul, J.; Movileanu, L. Single-Molecule Observation of Protein Adsorption Onto an Inorganic Surface. *J. Am. Chem. Soc.* **2010**, *132*, 10816–10822.
48. Carr, R.; Comer, J.; Ginsberg, M. D.; Aksimentiev, A. Microscopic Perspective on the Adsorption Isotherm of a Heterogeneous Surface. *J. Phys. Chem. Lett.* **2011**, *2*, 1804–1807.
49. Balan, A.; Machielse, B.; Niedzwiecki, D.; Lin, J.; Ong, P.; Engelke, R.; Shepard, K. L.; Drndić, M. Improving Signal-to-Noise Performance for DNA Translocation in Solid-State Nanopores at MHz Bandwidths. *Nano Lett.* **2014**, *14*, 7215–7220.
50. Wanunu, M. Nanopores: a Journey Towards DNA Sequencing. *Phys. Life Rev.* **2012**, *9*, 125–158.